Abundance and Sex Composition of Moose on the lower Kenai Peninsula, Alaska

Report by:

Daniel R. Eacker, Lead Consultant

Taurus Wildlife Consulting

Rick Merizon, Tribal Wildlife Biologist

Chugach Regional Resource Commission

Dustin Carl, Tribal Fish and Wildlife Dept. Director

Chugach Regional Resource Commission

September 10, 2026

CHUGACH REGIONAL RESOURCES COMMISSION

Aluutiiq Pride

TAURUS WILDLIFE CONSULTING

Table of Contents

List of Tables

List of Figures

EXECUTIVE SUMMARY

Accurate estimates of population abundance and sex composition are critical for sustainable population management, particularly for subsistence species subject to strict harvest limitations. In southern Game Management Unit (GMU) 15C, near the communities of Port Graham and Nanwalek, Alaska, management decisions for moose have historically relied on minimum aerial counts. These counts are uncorrected for sightability bias in dense coastal forest canopies. To address uncertainty surrounding local population status, we deployed a network of motion-triggered game cameras between August 2024 and April 2026. Binomial-mixture models were used in a Bayesian framework to estimate moose abundance, sex ratios, calf recruitment, and ecological drivers of space use during summer 2025. Our camera array yielded an estimated adult population of 23 moose (21 females, 2 males; 95% BCI = 12–75) across the 293.3 km^2 study area, corresponding to a low density of 0.1 moose/km^2. Encounter rates were heavily female-skewed (61% vs. 20% for males), resulting in an estimated bull:cow ratio of 8:100. This is well below the Alaska Department of Fish & Game typical statewide objective of 20–25 bulls per 100 cows used for a population managed for sustained harvest. Furthermore, recruitment was severely constrained, with only 3 subadult (yearling) detections and zero calves observed across all photos. Moose abundance was strongly concentrated at sites with high percentage of habitat availability and fresh water, while showing a strong negative relationship with black bear abundance. Notably, a single site characterized by 91% moose habitat availability (composed of herbaceous cover, broadleaf forest, and tall shrub communities) captured 74% of all moose detections. Given that local harvest is already strictly capped under permit hunt TM549 (3 bulls), the observed low density and poor recruitment appear driven by localized top-down predation and environmental constraints rather than hunter harvest. While camera surveys provided valuable baseline population insights without requiring marked individuals, standardizing camera viewshed measurements in future monitoring efforts would enable more accurate density estimation. Wildlife managers should prioritize the protection of key habitat stands and evaluate predator-prey dynamics to support local population resilience.

Keywords: Alces alces, black bear, habitat, harvest, recruitment, remote cameras, sex ratios, subsistence hunting, ungulate, *Ursus americanus*.

INTRODUCTION

Accurate estimates of population abundance and sex composition are fundamental for the sustainable conservation and management of game species, particularly in regions where local communities depend on subsistence resources. In the remote native communities of Port Graham and Nanwalek on the southern Kenai Peninsula in Southcentral Alaska, moose (*Alces alces*) represent a critical ecological and cultural resource (Carl et al. 2026). However, managing for hunter opportunity is challenging due to changing climatic conditions and perceived changes in moose movement and rut timing. These changes make it increasingly difficult for local hunters to safely navigate the terrain and harvest game within historic seasonal timelines. Furthermore, tribal members have voiced growing concerns over habitat pressure and direct resource competition from predators and commercial interests. In response to these issues, the Chugach Regional Resources Commission (CRRC) successfully advocated to adjust Game Management Unit (GMU) 15C hunting season closures, extending the window to November 30 to adapt to these contemporary challenges. However, because of the perception of low moose density, harvest is limited to three moose within the subsistence use area (TM549). Outside of TM549, Tribal community hunters are required to follow the state general season regulations that apply across Unit 15C (Carl 2026). Thus, reliable data on moose population abundance and sex composition (e.g., bull-to-cow ratios) are needed to inform moose harvest management decisions in this region.

Monitoring moose populations in coastal temperate rainforests presents significant logistical and technical challenges. Historic minimum counts by the Alaska Department of Fish & Game (ADF&G) highlighted low detected numbers of moose in the southern portion of GMU 15C, but these aerial survey techniques have been limited by dense forest canopy cover, steep fjord topography, maritime weather conditions, and restricted access across remote landscapes (Kellie et al. 2019). In spring 2024, the CRRC conducted an independent aerial survey within the Seldovia count area (includes TM549 hunt area and areas immediately north) and counted 21 adults and 1 calf moose. However, due to low detection rates, ADF&G estimates that up to 30% of the moose may be missed during aerial surveys in this area. Thus, there is considerable uncertainty in moose abundance in the region. Non-invasive sampling methodologies, particularly automated motion-triggered game camera networks, offer a potential cost-effective alternative for monitoring cryptic or low-density wildlife populations across challenging terrain (Palencia et al. 2021, Chaudhuri et al. 2022). For instance, Keever et al. (2017) demonstrated the utility of estimating abundance in a closed system using counts of unmarked white-tailed deer (*Odocoileus virginianus*) from game camera images. When combined with hierarchical modeling frameworks—such as binomial-mixture models (i.e., N-mixture models; Royle 2004)—

camera trapping count data can effectively account for imperfect detection while estimating spatially explicit site abundance across distinct habitat types and environmental gradients (Harris et al. 2024).

Beyond estimating moose abundance and sex composition, it is important to understand the ecological drivers of spatial variation in moose populations. These ecological drivers for moose include access to forage, proximity to fresh water, and refuge from predators. Forage availability, particularly early-seral browse, such as willow (*Salix* spp.), birch (*Betula* spp.), and aspen (*Populus tremuloides*) is a primary determinant of moose distribution and carrying capacity. These nutrient-rich species directly influence body condition and calf survival (Peek 1974, Franzmann and Schwartz 1985). Proximity to freshwater features, including riparian zones, lakes, and wetlands, provide both aquatic vegetation rich in essential minerals and critical microclimates for summer thermoregulation (MacCracken et al. 1993, van Beest et al. 2012). Concurrently, predation pressure exerts a strong top-down influence on space use, forcing moose to trade off optimal foraging habitats for thermal cover and dense canopy closure that offer spatial refuge during sensitive periods like calving and early summer (Bowyer et al. 1999, Hebblewhite and Merrill 2009, Francis et al. 2020). Thus, exploring these bottom-up and top-down influences can result in a more robust understanding of spatial variation in moose abundance.

We initiated a study in the southern Kenai Peninsula using automated game cameras in a binomial-mixture modeling framework to estimate moose abundance, sex composition, and recruitment to inform management of the resource. In addition to moose abundance and sex composition, we estimated moose densities based on prior information of adult female and male home range sizes (Cederland and Sand 1994, Thompson et al. 2024). We also accounted for site-level ecological covariates that could explain spatial variation in moose abundance. Because the region is generally considered poor habitat for moose (R. A. Merizon, personal communication, 15 August 2026), we first predicted that moose abundance would have a strong, positive correlation with the percent of available habitat, which we considered to be herbaceous cover, broadleaf forest, and open- and closed-canopy tall shrubs that moose would target for forage. Secondly, we predicted that moose abundance would be greater for sites that were closer to fresh water such as lakes and streams that provide aquatic vegetation and cover for thermoregulation. Finally, because black bears (*Ursus americanus*) are a known predator of moose calves (Ballard 1992), we predicted that moose abundance would be greater at sites with lower black bear abundance. In summary, our game camera study aimed to provide the first-ever moose abundance, sex composition, and recruitment estimates

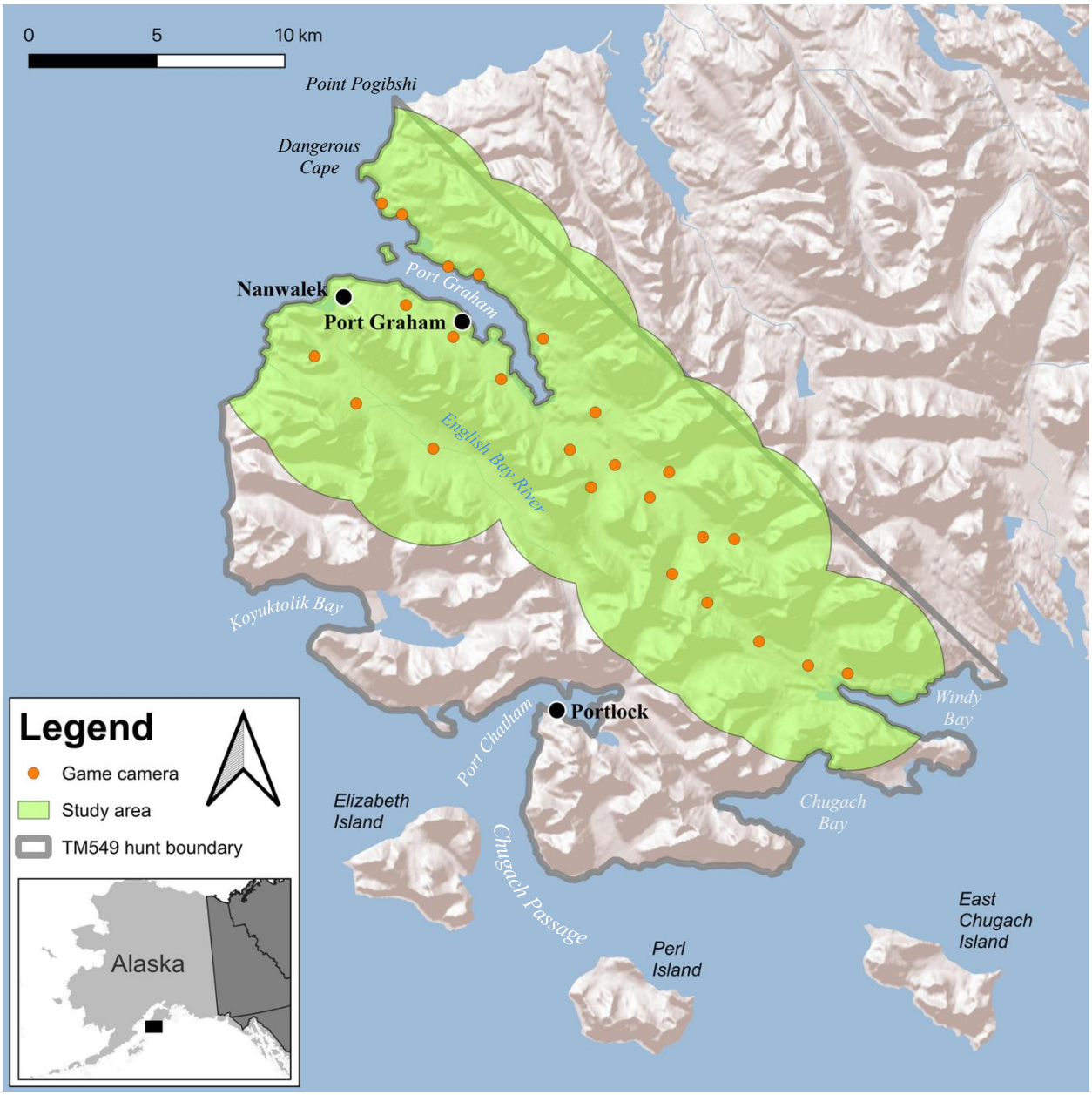

Figure 1. Port Graham study area showing the placement of 24 game cameras (orange points) and the 239.3 km^2 study area (green polygon) used for moose abundance estimation on the southern tip of the Kenai Peninsula, Alaska. Note that three cameras were not used in the analysis because they were not active during the analysis period of 15 June 2025 to 15 July 2025.

adjusted for imperfect detection in the region and explore relationships between moose abundance and key ecological covariates.

STUDY AREA

Our study occurred on the southwestern tip of the Kenai Peninsula near the communities of Port Graham and Nanwalek (59.3006° N, −151.7382° W) in Southcentral Alaska, USA,

and encompassed an area of 293.3 km^2 (Fig. 1). Elevation in the study area ranged from sea level to 1,202 m. The region is characterized by a glaciated maritime fjord landscape with topography that transitions rapidly from exposed bedrock headlands, intertidal gravel beaches, and low-lying estuarine marshes to steep coastal bluffs. The region experiences a subarctic, hyper-maritime climate marked by cool summers, relatively mild winters, heavy cloud cover, and high annual precipitation. This consistent precipitation regime feeds a network of flash-prone, high-gradient coastal streams emptying directly into Port Graham and English bays. During our study (15 June–15 July 2025), daily precipitation totaled 25.3 mm compared to a climate normal median of 36.8 mm (2002–2026); average daily temperatures fluctuated between 8.9°C and 15.0°C and climate normals averaged 8.4°C and 15.6°C between 2007–2026 (National Centers for Environmental Information [NCEI], 2026).

Situated within the northern extent of the Pacific coastal temperate rainforest ecoregion, the upland vegetation is heavily dominated by mature and secondary Sitka spruce (*Picea sitchensis*) canopy. The forest understory is dense and persistent, thick with devil's club (*Oplopanax horribilis*), salmonberry (*Rubus spectabilis*), Sitka alder (*Alnus viridis sinuata*), ferns, and deep moss ground cover. These forest communities grade into riparian corridors and coastal wetland areas, while the adjacent marine interface supports productive kelp beds and rich intertidal zones. Surrounding lands are primarily managed by native village and regional corporations (Port Graham Corporation and Cook Inlet Region, Inc.), where land use is low-intensity and largely focused on traditional Alutiiq/Sugpiaq subsistence harvesting, small-scale forestry, and wildlife habitat preservation, with regional access restricted to a short road system, marine vessels, and small aircraft.

Mammalian populations detected on camera in the study area included moose, black bear, coyote (*Canis latrans*), wolverine (*Gulu gulu*), feral dog (*Canis familiaris*), Canadian lynx (*Lynx canadensis*), snowshoe hare (*Lepus americanus*), American marten (*Martes americana*), and red squirrel (*Tamiasciurus hudsonicus*; see Appendix S1).

METHODS

Camera deployment logistics occurred with Port Graham and Nanwalek Tribal councils, village corporations, and the regional corporation on a 2 km^2 grid over the study area. Given the limited access, 27 cameras were placed adjacent to the road and trail systems of Port Graham and Nanwalek. We attempted to deploy each camera trap as close as possible to the center of each grid cell. At each camera location, a camera viewshed was identified to maximize sightability (i.e., >5 m), and grass and small brush were cleared within the viewshed of the camera to avoid falsely triggering cameras. Cameras were secured to a

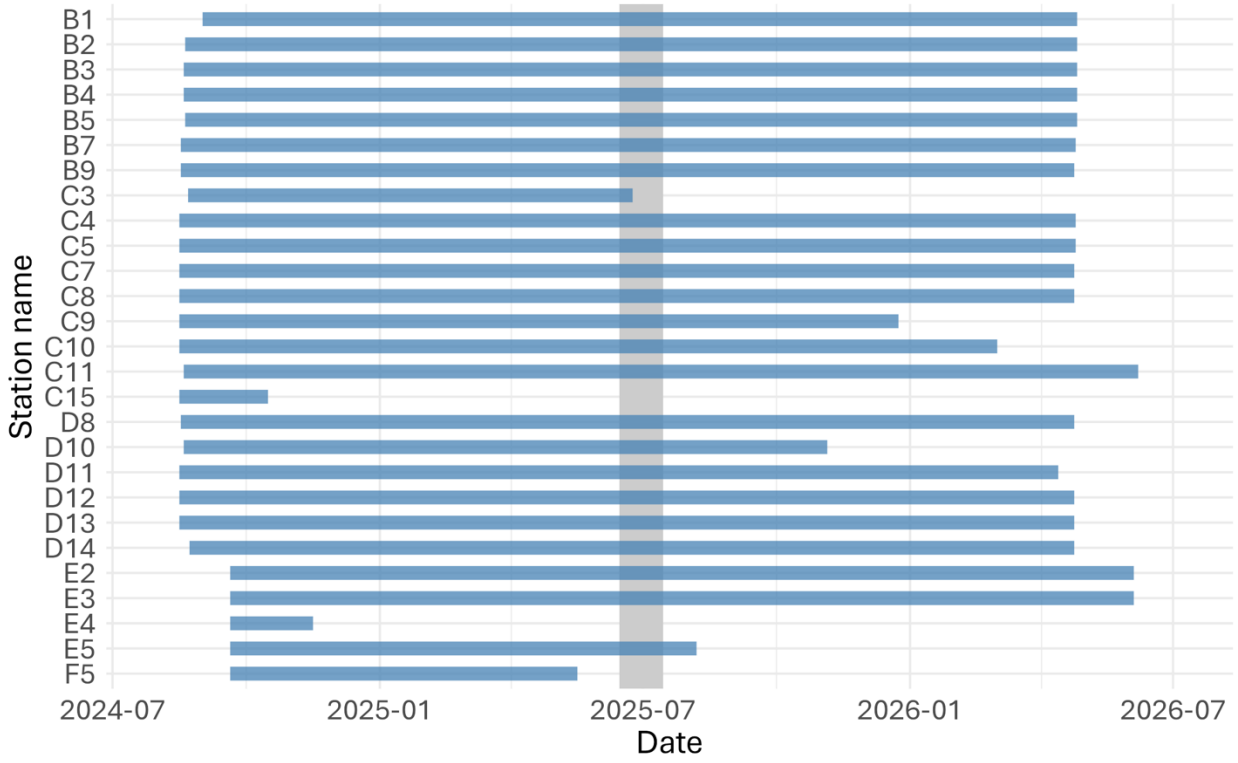

Figure 2. Camera station operational periods for 27 game cameras set up for moose abundance estimation on the southern tip of the Kenai Peninsula in Alaska during 16 August 2024 to 7 June 2026. Note that 3 cameras (i.e., C15, E4, and F5) were not included in the analysis that did not have coverage over the analysis period from 15 June 2025 to 15 July 2025 (shown in gray shading).

tree ≥10 cm in diameter using a strap at 1.5 m in height above ground. Browning Dark OpsMax HD motion-sensing game cameras were used (Prometheus Group LLC, Birmingham, Alabama, USA) with 64 GB memory cards and 8–10 lithium AA batteries. Cameras were set to collect a single image upon motion detection trigger both day and night and to allow 12–15 months between visits. Both batteries and SD memory cards were changed during each visit.

We used the AddaxAI interface (Van Lunteren 2023) to apply MegaDetector (Beery et al. 2019) and Google Species Net (Gadot et al. 2024) models to process our photos from automated game cameras, which are image recognition models used for detection and species classification, respectively. Then, we used the resulting image recognition file in Timelapse (Greenburg et al. 2019), an open-source data management software, to tag all images and extract photo metadata. As a conservative measure, we classified moose as unknown sex if we did not have high confidence in the classification.

Following a recent moose abundance study (Boone et al. 2025), we restricted our analysis to a 30-day period in early summer 2025 to avoid moose breeding behavior biasing adult male detections high due to increased seasonal movement rates, for instance, in the

rut. Thus, our analysis period was defined from 15 June 2025 to 15 July 2025 when overall detection rates were high (Fig. 3), but movement rates were more similar between the sexes. We used 15-minute intervals to define independent detections of moose and calculated the maximum number of adult male, adult female, and unknown sex moose observed in each interval. This relatively short interval prevented a moose from being detected, for example, as an adult male and unknown sex moose within the same interval. We then summed these counts over days to create encounter histories. Because not all cameras were operational over the full 30-day period (Fig. 2), we created a matrix for trap operation to account for variable availability to detect moose.

Ecological Covariates

We considered ecological covariates to explain variation in moose abundance including percent of available moose habitat, distance from water (i.e., lakes and streams), and black bear abundance. We first extracted vegetation data from the Kenai Peninsula Existing Vegetation Map layer (USFS 2020) that provides habitat classification data on dominant vegetation type, tree canopy cover, tree size, and tall shrub canopy cover. In collating this variable, we filtered vegetation polygons for dominance types of herbaceous cover, broadleaf forest, and tall shrubs, and then further filtered tall shrubs for open (25%–59% shrub cover) and closed (60%–100% shrub cover) tall shrub canopies. We then clipped the resulting polygons by 50-m, 250-m, and 1,000-m buffers around camera sites and calculated the percent of available moose habitat within each buffer. Because moose spend much of their time along streams and lakes where preferred forage is abundant, we considered distance to water as a covariate to explain moose abundance (U.S. Fish and Wildlife Service 2006). We used the package 'sf' (Pebesma 2018, Pebesma and Bivand 2023) in Program R (R Core Team 2025) to process moose habitat and distance to water covariates. Finally, we estimated abundance of black bears to use as a predictor of moose abundance. We used a similar approach to our moose abundance model except without covariates on abundance and no sex-specificity (see below).

Statistical Inference

We used the package 'nimble' (de Valpine et al. 2017, de Valpine et al. 2026) in R (R Core Team 2025) to conduct Markov chain Monte Carlo (MCMC) sampling and produce posterior samples of latent parameters (e.g., abundance and detection probability) for binomial-mixture models (see Appendix S2 for full model description). We also used 'nimble' (de Valpine et al. 2017, de Valpine et al. 2026) to carry out Bayesian model selection and averaging using reversible-jump MCMC (Green 1995), which samples through parameter spaces of varying dimensions and provides relative support for candidate models and target parameters simultaneously using a set of indicator variables.

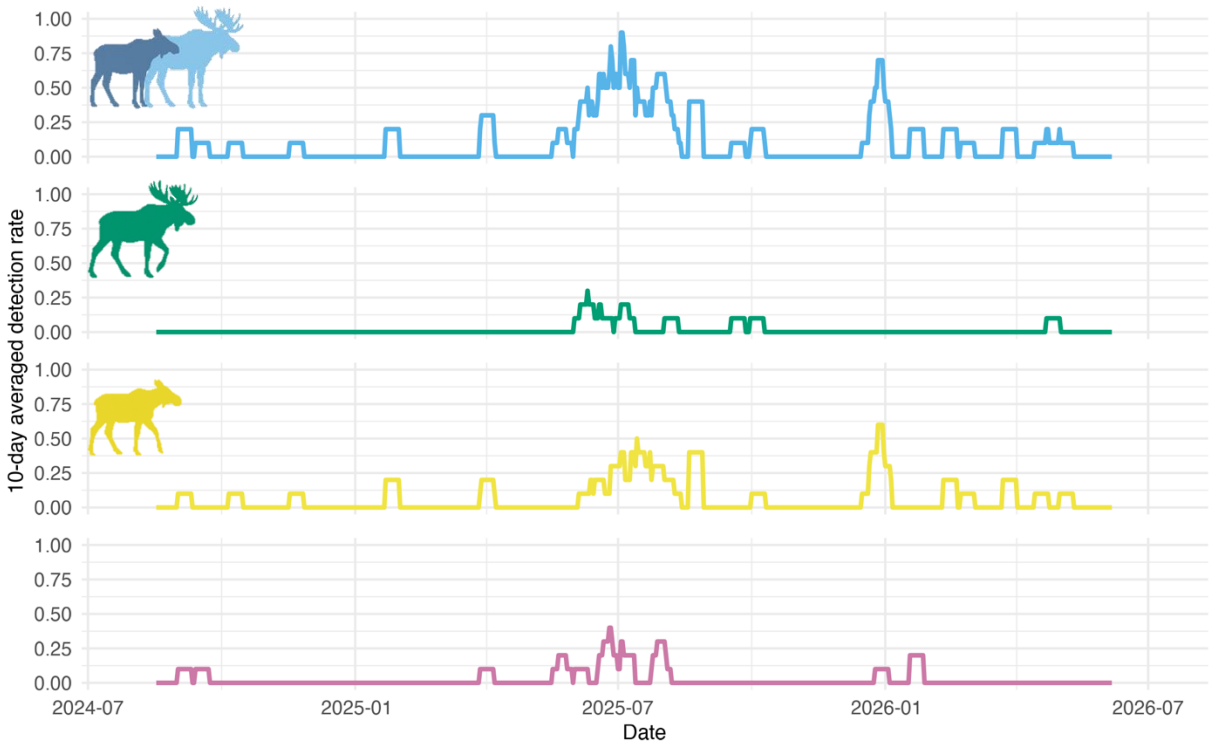

Figure 3. Moose detection rates from game cameras using a 10-day moving average for all moose (blue), adult male (green), adult female (yellow), and unknown sex moose (reddish purple) on the southern tip of the Kenai Peninsula in Alaska during 16 August 2024 to 7 June 2026. Note that counts were based on the maximum number of individuals of each sex class observed in 15-minute intervals and then summed over days.

Additionally, we compared the Watanabe-Akaike information criterion (WAIC), which provides a metric to compare single models in a Bayesian framework with lower values indicating greater model support (Watanabe 2010). We considered variables as important predictors if their 95% Bayesian credible intervals (BCI) did not overlap zero. We screened for collinearity by examining correlation among continuous covariates and only included variables with correlation coefficients <|0.7| (Dormann et al. 2013). We standardized continuous variables by centering and scaling by one standard deviation to allow comparison of relative effect sizes. We ran at least 2 MCMC chains for 50,000 iterations with a 10,000 burn-in interval for a total of 40,000 samples per chain. As standard checks of MCMC convergence, we visually inspected trace plots of posterior samples for adequate mixing and estimated the Brooks-Gelman-Rubin statistic and confirmed that it was <1.1 (Gelman and Rubin 1992, Brooks and Gelman 1998). Further, we conducted posterior predictive checks by using the parameter values in the model to generate new data and calculate a chi-squared discrepancy statistic (Kéry and Schaub 2012). A Bayesian *p*-value of 0.5 indicated no discrepancy between the observed and replicated datasets and suggested the model could generate the observed data. We collated our image tag data and conducted all analyses in Program R (R Core Team 2025).

Finally, as an estimate of density, we divided sex-specific abundance estimates by a circular home range size for male and female moose. Although no moose home range studies exist for GMU 15C, a recent moose forage ecology study on the Kenai Peninsula estimated an adult female home range size of 16.2 km^2 during lactation (Thompson et al. 2024). Thus, we used a home range size of 15 km^2 for adult female and 30 km^2 for adult male moose, assuming adult males would have twice as large of a home range size (Cederland and Sand 1994). This resulted in sex-specific study areas of 218.5 km^2 for adult females and 293.3 km^2 for adult males under a bivariate normal model of space use.

RESULTS

We captured a total of 37,321 photos from 27 cameras between 26 August 2024 and 7 June 2026. However, 98% of these photos were empty due to wind trigger events from tall grass. Of photos containing wildlife, 34% were moose, 26% were black bear, 20% were coyote, 8% were unknown species, 5% were birds, 3% were wolverine, 1% were domestic/feral dog, 1% were Canadian lynx, 1% were red squirrel, and less than 1% were snowshoe hare and American marten. After removing 3 cameras that were not operational during our analysis period (see Fig. 2), our dataset included 24 cameras. Adult female moose had higher encounter rates than adult males, with 61% of images being adult females, 20% being adult males, and 19% being unknown sex with most detections occurring over summer (Fig. 3). Only 3 out of 159 moose photos with identifiable age class were classified as subadult (i.e., yearling) and none were juveniles. Out of 33 images where adult male antlers could be classified, 91% were in velvet and 9% were hardened. No trophy-class adult males (≥125cm / 50 in total antler spread) were observed. One camera had the majority (74%) of moose detections over our 30-day analysis period.

In our moose abundance analysis, we retained the 50 m buffer for percent of available moose habitat because it had the strongest correlation with moose abundance out of the buffers considered. All models converged based on visual inspection of trace plots and Brooks-Gelman-Rubin statistics being <1.1. All predictor variables were significant in both univariate and multivariate models given that their 95% Bayesian credible intervals (BCI) did not overlap zero (Table 1). We detected no issues with collinearity between predictor variables based on correlation coefficients $<|0.7|$ and that coefficient estimates were stable across univariate and multivariate models (Table 1).

We found overwhelming support for the model that included all three predictor covariates (see Table 2). We found no evidence that the model could not generate the observed data (Bayesian *p*-value = 0.44). As predicted, we found that moose abundance increased with increasing levels of percent of available habitat, decreased with increasing

Table 1. Standardized coefficient estimates with 95% Bayesian credibility intervals (BCI) for percent of available moose habitat (habitat), distance to water (water), and bear abundance (bear) from univariate and multivariate binomial-mixture models of moose abundance.

	Univariate		Multivariate	
Coefficient	$\hat{\beta}$(SD)	95% BCI	$\hat{\beta}$(SD)	95% BCI
$\beta_{habitat}$	0.79 (0.25)	0.31, 1.28	1.08 (0.25)	0.62, 1.59
β_{water}	−1.04 (0.55)	−2.27, −0.15	−1.29 (0.54)	−2.61, −0.52
β_{Bear}	−1.96 (1.72)	−6.62, −0.11	−2.63 (1.65)	−7.00, −0.86

Table 2. Model selection for the top 4 of 8 nested models showing posterior model probabilities (ω_M) from Bayesian reversible-jump Markov chain Monte Carlo and WAIC using weakly informative Cauchy(0, 2.5) priors for regression coefficients representing the effects of percent of available moose habitat (habitat), distance to water (water), and bear abundance (bear) on moose abundance from binomial-mixture models. Note that the covariate will have a 1 in the table if it is present in the model.

	Covariate				
Model	Habitat	Water	Bear	ω_M	WAIC
8	1	1	1	0.994	140.4
6	1	0	1	0.004	144.2
5	1	0	0	0.001	145.0
7	1	1	0	0.001	144.4

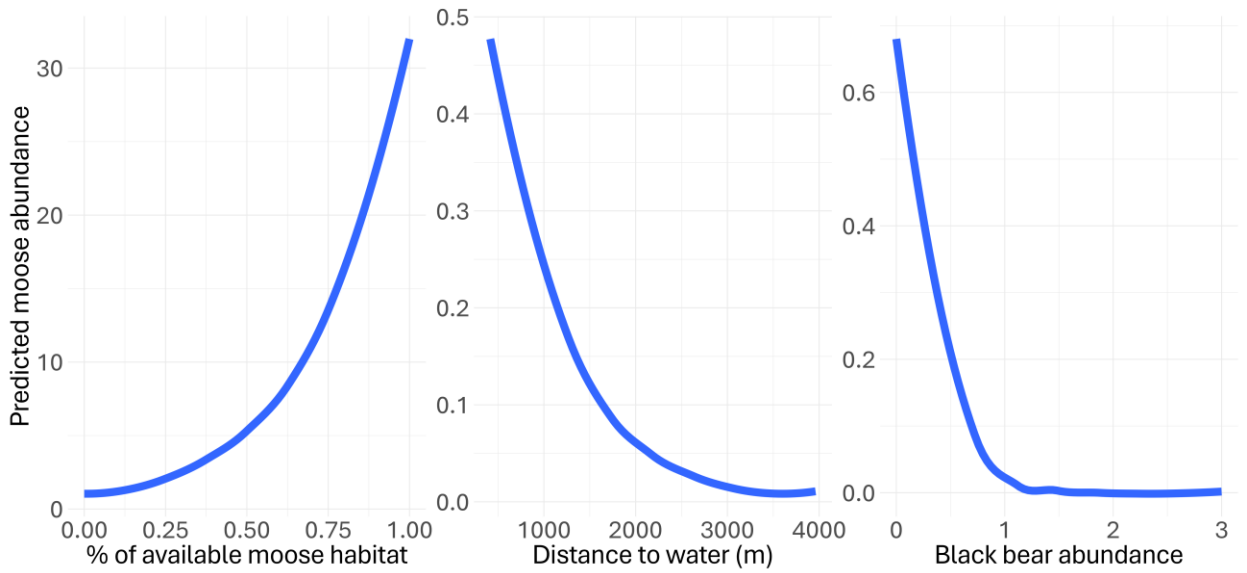

Figure 4. Predicted moose abundance from binomial-mixture models over the range of observed covariates for percent of available moose habitat, distance to water (m), and black bear abundance on the southern tip of the Kenai Peninsula in Alaska during 15 June 2025 to 15 July 2025. Note the difference in the scale of y-axis among the different panels.

distance from water, and decreased with increasing black bear abundance (Fig. 4). The model-averaged estimate of total moose abundance was 23 (95% BCI = 12, 75) with a sex ratio of 8 (95% BCI = 2, 40) adult males per 100 adult females. We estimated a total of 21 (95% BCI = 10, 73) adult female and 2 (95% BCI = 1, 8) adult male moose. Sex-specific

abundance estimates translated into densities of 0.095 (95% BCI = 0.044, 0.334) adult female moose/km^2 and 0.005 (95% BCI = 0.004, 0.026) adult male moose/km^2. Average baseline detection probabilities were around 3–4 times higher for adult males (p_0 = 0.11, 95% BCI = 0.02, 0.26) compared to adult females (p_0 = 0.03, 95% BCI = 0.01, 0.08) and moose with unknown sex (p_0 = 0.04, 95% BCI = 0.01, 0.10); these per occasion detection probabilities translated into cumulative probabilities (i.e., the probability of detecting at least one individual) of 0.97 (95% BCI = 0.51, 1.00), 0.57 (95% BCI = 0.17, 0.90), and 0.67 (95% BCI = 0.21, 0.96), respectively. While standardized black bear abundance and distance to water had the strongest relative effect sizes per standard deviation (Table 1), the unstandardized prediction curves highlight the contrasting ecological importance of our covariates. Across its full observed range, percent of available moose habitat yielded a noticeably larger shift in predicted moose abundance (increasing from near zero to over 30 individuals) compared to the effects of distance to water and black bear abundance, which altered predicted abundance by less than one individual (Fig. 4).

To estimate black bear abundance, we found that a model that assumed a zero-inflated Poisson process for abundance was slightly more supported (WAIC = 97.6) and fit the data better (Bayesian p = 0.32) than a simple Poisson distribution (WAIC = 98.1, Bayesian p = 0.30). The total estimated black bear abundance was 9 bears (95% BCI = 6, 37). The zero-inflated model estimated that only 35% of sites were suitable for black bears, which was expected because only 4 out of 24 sites had detections during the analysis period. The average baseline detection probability per occasion was 0.05 (95% BCI = 0.01, 0.11) with a cumulative detection probability of 0.81 (95% BCI = 0.32, 0.97).

DISCUSSION

Estimating population abundance and sex composition is fundamental for sustainable harvest management of game species, especially in areas with considerable uncertainty in population status. Our game camera study provided key insights into the moose population within the TM549 management area of GMU 15C that minimum counts from aerial surveys traditionally miss. These insights included adjusting abundance and sex composition estimates for imperfect detection and identifying ecological correlates of moose abundance in the study area. Adult female moose exhibited substantially higher encounter rates than males (61% vs. 20%) in game camera photos, and a sex ratio of 8 bulls:100 cows indicated a population with limited harvest potential. Notably, recruitment appeared critically constrained in the population, with only 3 of 159 moose images classified as subadults (yearlings) and no juveniles (calves) observed in any photos. Also, we observed a pronounced spatial concentration where a single camera site captured 74% of all moose detections during the sampling period.

Demographic estimates from our study place the moose population in the TM549 management area of GMU 15C at the lower extreme of density and bull-to-cow ratios recorded across coastal Alaska. We estimated a total of 23 adult moose (21 females and 2 males) in our study area between 15 June–15 July 2025. During the aerial survey completed in March 2024, a minimum count of 4 moose was documented in this same study area. This discrepancy can potentially be explained by the fact that minimum counts are not corrected for sightability, and that the assumed 70% detection rate for this area estimated by ADF&G is biased severely high. However, our estimated abundance falls within the minimum counts of 10 to 48 moose reported by ADF&G over 2011 to 2017 for this area. It should be noted, ADF&G's Seldovia minimum count area is larger and has observed higher bull:cow ratios than this study. The sex ratio estimated from our binomial-mixture models (8 bulls:100 cows) falls well below the management objective in GMU 15C of 20 to 25 bulls per 100 cows to ensure adequate breeding coverage and preserve harvest opportunity (Herreman 2022). Moose densities in Alaska can range from 0.013 moose/km^2 to over 1.93 moose/km^2 (ADF&G [n.d.]), and our combined density estimate was at the lower end of this range at 0.1 moose/km^2. Along with the general sparsity of moose in our study area, our density estimate is expected to be lower in summer as most moose density estimates are based on winter range when moose are concentrated due to deep snowpack. For example, moose on the Gustavus Forelands in Southeastern Alaska on their winter range were recorded at some of the highest densities in Alaska at around 3.9 moose/km^2 (White et al. 2004). Thus, combined with evidence of low recruitment, the low-density moose population in the southern portion of GMU 15C appears strongly constrained by localized environmental limits.

Spatial variation in moose abundance across our study area was strongly shaped by a combination of habitat availability, proximity to water, and presence of black bears. As predicted, moose abundance responded positively to the availability of habitat and proximity to fresh water. During early summer, early seral browse species such as willow (*Salix* spp.) and birch (*Betula* spp.) provide the high-protein forage necessary to support body condition, while riparian corridors offer essential aquatic vegetation for mineral intake alongside critical microclimates for thermoregulation (MacCracken et al. 1993, van Beest et al. 2012). Notably, only two of our sites had available moose habitat percentages above 32%, with the single camera site that recorded the majority of moose detections having 91% of available moose habitat; this site also had one of the lowest distances to fresh water at 843 m. Conversely, moose abundance decreased in areas with higher black bear abundance. Black bears can exert strong top-down pressure on moose populations in coastal Alaska through direct calf predation, especially where brown bears (*Ursus arctos*) are uncommon (Ballard 1992). Given that we detected zero calves or brown bears during

our sampling period, this strong negative relationship with black bear abundance highlights how predation risk—or risk-sensitive behavioral avoidance—can heavily constrain localized space use and recruitment in low-density populations. Additionally, although not evaluated in our analysis, coyotes were frequently detected across our study sites (20% of wildlife detections); while primarily scavengers, coyotes can occasionally prey on neonate moose calves (Benson and Patterson 2013). Collectively, these habitat trade-offs and predator dynamics suggest that localized environmental constraints dictate space use.

Several methodological limitations warrant consideration when evaluating these results. First, because we lacked empirical movement and space-use data from GPS-collared moose in our study area, density estimates were derived using prior information from another study (Thompson et al. 2024) and should be interpreted cautiously. Second, 19% of moose images could not be definitively classified by sex, requiring us to apportion unclassified individuals based on the estimated proportion of adult males and females. While this introduced minor uncertainty into sex ratios, our binomial-mixture models explicitly corrected adult male and female abundances for imperfect detection when estimating the overall sex ratio. Third, two camera sites with moose detections were separated by only 3.4 km, introducing the possibility of double-counting given typical moose movement distances. However, because one of these sites recorded only a single detection while the other captured the vast majority of photos, double-counting likely imparted minimal bias on total abundance estimates. Finally, documented correlations between ecological covariates and moose abundance were heavily driven by the single camera location that dominated detections. Beyond habitat availability, proximity to water, and low bear activity, unmeasured micro-site characteristics may further explain this high concentration of use.

From a management perspective, our findings provide context for interpreting local population status and establishing realistic monitoring expectations in southern GMU 15C. Although harvest is already strictly capped under permit hunt TM549 (3 bulls), our estimated sex ratio of 8 bulls per 100 cows—combined with the complete absence of detected calves—indicates that low density and poor recruitment are likely driven by top-down predation or low calf survival rather than hunter harvest. Furthermore, while formal recalibration of aerial survey sightability would require GPS-collared animals, managers should recognize that the standard 70% detection assumption could underestimate true abundance in the dense coastal canopy, meaning minimum aerial counts should be treated as conservative indices rather than absolute population sizes. Finally, if localized camera monitoring is conducted in the future, measuring individual camera viewsheds and effective sampling areas would enable more accurate estimation of moose density (e.g., space-to-event models, Moeller et al. 2018) without requiring long-term study

commitments. Given the low moose density across the area, management efforts may be most effectively focused on preserving high-quality riparian habitats and monitoring predator-prey dynamics rather than maintaining intensive population estimation infrastructure.

ACKNOWLEDGEMENTS

The authors are very grateful for all the support they received before, during, and after this project was completed. Specifically, we thank the following for their support: N. Fowler with developing the grid array for camera deployment. B. Hetrick, B. Buzby, M. Lee, and H. Hellen for camera deployment, visits, and SD card recovery. Numerous community members of Port Graham and Nanwalek provided many hours of support including V. Malchoff and Q. McMullen. Finally, we thank J. Herreman for the providing a review of our manuscript.

LITERATURE CITED

Alaska Department of Fish and Game. 2026. Moose hunting in Alaska. Alaska Department of Fish and Game, Juneau, USA. https://www.adfg.alaska.gov/index.cfm?adfg=moosehunting.moremoose. Accessed 2 Sep 2026.

Ballard, W. B. 1992. Bear predation on moose: a review of recent North American studies and their management implications. Alces Supplement 162–176.

Beery, S., D. Morris, and S. Yang. 2019. Efficient pipeline for camera trap image review. arXiv preprint arXiv:1907.06772.

Benson, J. F., and B. R. Patterson. 2013. Moose (*Alces alces*) predation by eastern coyotes (*Canis latrans*) and eastern coyote × eastern wolf (*Canis latrans* × *Canis lycaon*) hybrids. Canadian Journal of Zoology 91:837–847.

Boone, H., M. Romanski, K. Kellner, R. Kays, L. Potvin, G. Roloff, and J. Belant. 2025. Optimal timing to estimate moose *Alces alces* demographic parameters using remote cameras. Scientific Report 15:20493.

Bowyer, R. T., V. Van Ballenberghe, and J. G. Kie. 1999. Habitat selection by female moose: effects of predation risk and food availability. Alces 35:41–56.

Brooks, S. P., and A. Gelman. 1998. Alternative methods for monitoring convergence of iterative simulations. Journal of Computational and Graphical Statistics 76:434–455.

Carl, D., C. Woodard, H. P. Huntington, and W. Hetrick-Price. 2026. Hunting and using moose (*Tegllit*) in Nanwalek and Port Graham, Alaska. Case Studies 2026:72–82. Chugach Regional Resources Commission, Anchorage, Alaska, USA. crrcalaska.org. Accessed 1 Sep 2026.

Cederlund, G., and H. Sand. 1994. Home-range size in relation to age and sex in moose. Journal of Mammology 75:1005–1012.

Chaudhuri, S., R. Rajaraman, S. Kalyanasundaram, S. Sathyakumar, and R. Krishnamurthy. 2022. N-mixture model-based estimate of relative abundance of sloth bear (*Melursus ursinus*) in response to biotic and abiotic factors in a human-dominated landscape of central India. PeerJ 10:e13649.

de Valpine, P., D. Turek, C. J. Paciorek, C. Anderson-Bergman, D. Temple Lang, and R. Bodik. 2017. Programming with models: writing statistical algorithms for general model structures with NIMBLE. Journal of Computational and Graphical Statistics 26:403–413.

de Valpine P., C. Paciorek C, D. Turek, N. Michaud, C. Anderson-Bergman, F. Obermeyer, C. Wehrhahn Cortes, A. Rodrìguez, D. Temple Lang, and S. Paganin. 2026. NIMBLE: MCMC, Particle Filtering, and Programmable Hierarchical Modeling. doi:10.5281/zenodo.1211190 <https://doi.org/10.5281/zenodo.1211190>, R package version 1.4.2, <https://cran.r-project.org/package=nimble>.

Dormann, C. F., J. Elith, S. Bacher, and C. M. Buchmann. 2013. Collinearity: a review of methods to deal with it and a simulation study evaluating their performance. Ecography 36:27–46.

Francis, A. L., C. Procter, G. Kuzyk, and J. T. Fisher. 2020. Female moose prioritize forage over mortality risk in harvested landscapes. Journal of Wildlife Management 85:156–168.

Franzmann, A. W., and C. C. Schwartz. 1985. Moose twinning rates: a possible population condition indicator. The Journal of Wildlife Management 49:394–398.

Gadot, T., S. Istrate, H. Kim, K. Morris, S. Beery, T. Birch, and J. Ahumada. 2024. To crop or not to crop: comparing whole-image and cropped classification on a large dataset of camera trap images. IET Computer Vision 18:1193–1208.

Gelman, A. and D. B. Rubin, D. B. 1992. Inference from iterative simulation using multiple sequences. Statistical Science 7:457–472.

Green, P. J. 1995. Reversible jump Markov chain Monte Carlo computation and Bayesian model determination. Biometrika 82:711–732.

Greenberg, S., T. Godin, and J. Whittington. 2019. Design patterns for wildlife-related camera trap image analysis. Ecology and Evolution 9:13706–13730.

Harris, G. M., D. R. Stewart, M. J. Butler, E. M. Rominger, C. Q. Ruhl, D. T. McDonald, and P. M. Schmidt. 2024. N-mixture models with camera trap imagery produce accurate abundance estimates of ungulates. Scientific Reports 14:13421.

Hebblewhite, M., and E. Merrill. 2009. Trade-offs between predation risk and forage differ between migrant strategies in a migratory ungulate. Ecology 90:3445–3454.

Herreman, J. 2022. Moose management report and plan, Game Management Unit 15: Report period 1 July 2015–30 June 2020, and plan period 1 July 2020–30 June 2025. Alaska Department of Fish and Game, Species Management Report and Plan ADF&G/DWC/SMR&P-2022-24, Juneau.

Keever, A. C., C. P. McGowan, S. S. Ditchkoff, P. K. Acker, J. B. Grand, and C. H. Newbolt. 2017. Efficacy of N-mixture models for surveying and monitoring white-tailed deer populations. Mammal Research 62:413–422.

Kellie, K. A., K. E. Colson, and J. H. Reynolds. 2019. Challenges to monitoring moose in Alaska. Alaska Department of Fish and Game, Wildlife Management Report ADF&G/DWC/WMR-2019-1, Juneau.

Kéry, M., and M. Schaub. 2012. Bayesian population analysis using WinBUGS: a hierarchical perspective. Academic Press, Boston, Massachusetts, USA.

MacCracken, J. G., V. Van Ballenberghe, and J. M. Peek. 1993. Use of aquatic plants by moose: sodium hunger or foraging efficiency? Canadian Journal of Zoology 71:2345–2351.

Moeller, A. K., P. M. Lukacs, and J. S. Horne. 2018. Three novel methods to estimate abundance of unmarked animals using remote cameras. Ecosphere 9(8):e02331.

National Centers for Environmental Information. 2026. Global Historical Climatology Network - daily (GHCN-Daily), version 3. National Oceanic and Atmospheric Administration. <https://www.ncei.noaa.gov/products/land-based-station/global-historical-climatology-network-daily>. Accessed 25 Aug 2026.

Palencia, P., J. Fernández-López, J. Vicente, and P. Acevedo. 2021. Innovations in movement and behavioral ecology from camera traps: Day range as model parameter. Methods in Ecology and Evolution 12:1201–1212.

Pebesma, E., and R. Bivand. 2023. Spatial data science: with applications in R. Chapman and Hall/CRC, London, UK.

Pebesma, E., 2018. Simple features for R: standardized support for spatial vector data. The R Journal 10:439–446.

Peek, J. M. 1974. A review of moose habitat research in North America. The Canadian Field-Naturalist 88:217–231.

R Core Team 2025. R: A Language and Environment for Statistical Computing. R Foundation for Statistical Computing, Vienna, Austria. https://www.R-project.org/.

Royle, J. A. 2004. N-mixture models for estimating population size from spatially replicated counts. Biometrics 60:108–115.

Schwartz, C. C., and A. W. Franzmann. 1989. Bears, wolves, moose, and forest succession, some management considerations on the Kenai Peninsula, Alaska. Alces 25:1–10.

Thompson, D. P., N. L. Fowler, J. A. Crouse, T. J. McDonough, O. H. Badajos, M. O. Spathelf, D. E. Watts, and S. U. Rodman. 2024. Seasonal somatic reserves of a northern ungulate influenced by reproduction and a fire-mediated landscape. Frontiers in Ecology and Evolution 12:1433485.

U.S. Fish and Wildlife Service. 2006. KP_Landcover_2002 version 2 vector digital data. Kenai National Wildlife Refuge, Lee O'Brien, GIS Manager. <\\lfw7ken-svr3\GIS\landcover\KP_Landcover_V1.shp>. Accessed 15 Aug 2026.

U.S. Forest Service. 2020. Kenai Peninsula Existing Vegetation Map. USDA Forest Service, Alaska Region. Available online via the Kenai Peninsula Existing Vegetation Hub.

van Beest, F. M., B. Van Moorter, and J. M. Milner. 2012. Temperature-induced habitat selection in a large herbivore facing climate warming. Journal of Animal Ecology 81:142–153.

Van Lunteren, P. 2023. AddaxAI: A no-code platform to train and deploy custom YOLOv5 object detection models. Journal of Open Source Software 8:5581.

Wantanabe, Sumio. 2010. Asymptotic equivalence of Bayes cross validation and widely applicable information criterion in singular learning theory. Journal of Machine Learning Research 11:3571–3594.

White, K. S., N. L. Barten, and J. A. Crouse. 2004. Effects of food-limitation on an irruptive, high-density moose population on the Gustavus Forelands, Alaska [abstract]. Page 59 [In] Program and abstracts of Predator-Prey 2004: Joint conference and annual meeting of the Northwest Section and Alaska Chapter of the Wildlife Society, 1-3 May 2004, Girdwood, Alaska.

APPENDIX

Appendix S1. Game camera images of mammalian species detected in study area including (A) black bear, (B) coyote, (C) wolverine, (D) feral dog, (E) Canadian lynx, (F) snowshoe hare, (G) American marten, and (H) red squirrel.

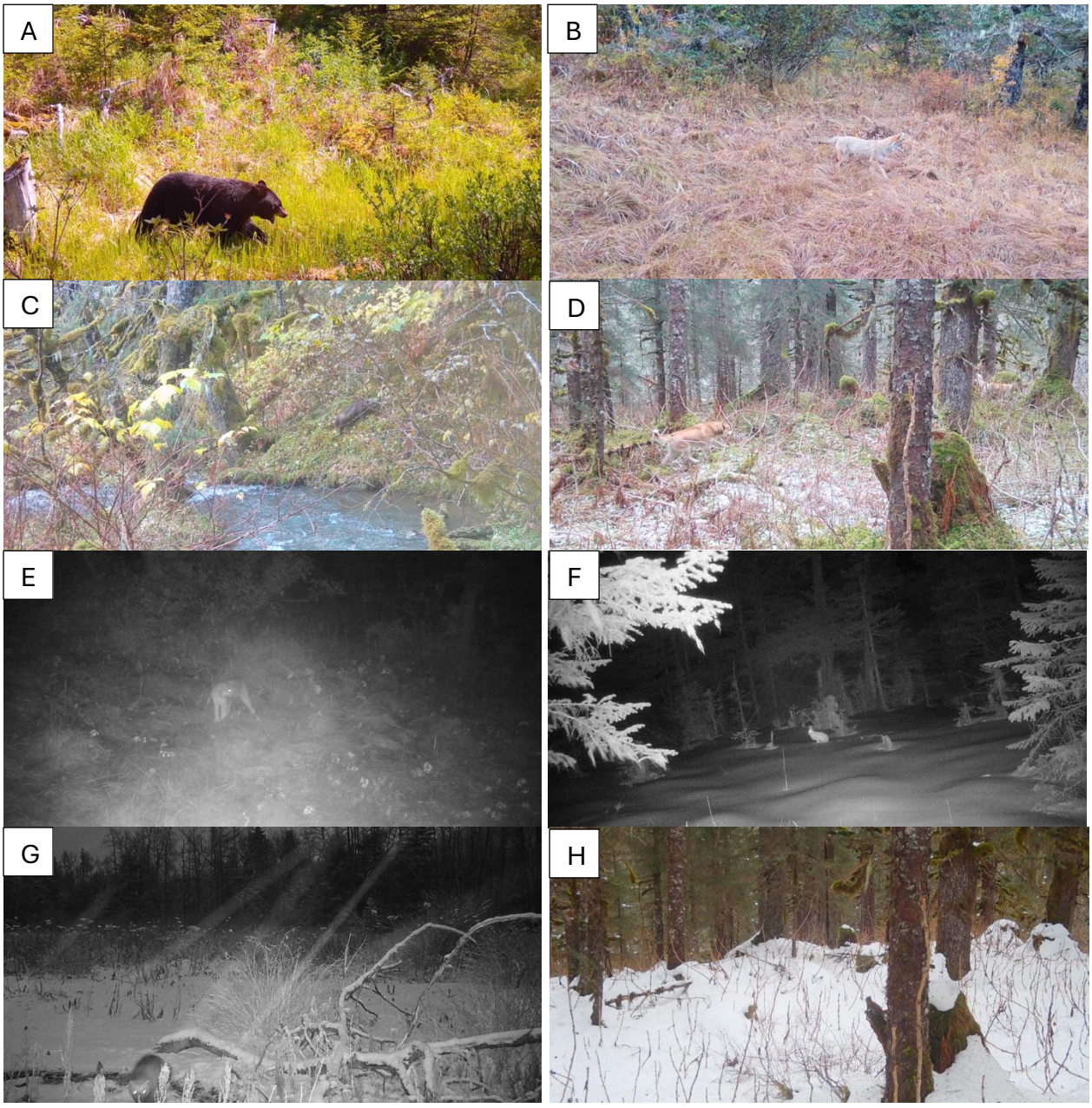

Appendix S2. Description and specification of Bayesian binomial-mixture model used to estimate moose abundance and sex composition from game camera images.

We used binomial-mixture models in a Bayesian framework to estimate the population size of moose from our spatially replicated counts at cameras sites (Royle 2004). Like other hierarchical approaches, the model includes an ecological process that yields a latent (unobserved) state and an observation process that yields observations. Thus, the spatial variation of local abundance at cameras site *i*, N_i, is described by a Poisson distribution with mean λ. We also considered a zero-inflated Poisson distribution of abundance to describe the latent abundance process, which estimates the probability (ψ) that a suite is suitable (z = 1) or not (z = 0) for a given species when there were excess zeros in count data. The observed counts y_{ij} (given N_i) at site *i* and during occasion *j* are described by a binomial distribution with sample size N_i and detection probability *p*. We also introduced a vector of site-level ecological covariates (***x***) using a log link function to explain variation in abundance and estimated baseline detection rates on the logit scale, which yields the model specification in the following equation:

$$
\begin{gathered}
N_{ik} \sim \text{Poisson}(\lambda_{ik}) \\
\log(\lambda_{ik}) = \alpha_0 + \alpha_k + \boldsymbol{x}_i^T \boldsymbol{\alpha} \\
y_{ijk} \sim \text{Binomial}(p_{ijk}, N_{ik}) \\
p_{ijk} = \begin{cases} \text{logit}^{-1}(\beta_{0,k}) & \text{if effort}_{ij} = 1 \\ 0 & \text{if effort}_{ij} = 0 \end{cases} \\
\alpha_0 \sim \mathcal{N}(0,10), \\
\alpha_k \sim \mathcal{N}(0,10),\ k = 1, \ldots, K \\
\alpha_p \sim \text{Cauchy}(0,2.5) \text{ for } p = 1, \ldots, P \\
\beta_{0,k} \sim \mathcal{N}(0,2) \text{ for } k = 1, \ldots, K
\end{gathered}
\tag{1}
$$

where we assume log intercepts on the overall grand mean (α_0) and sex-specific latent abundances (α_k) arose from independent Normal distributions (i.e., prior distributions) with mean 0 and variance 10, the vector of coefficients (***α***) explaining abundance arose from Cauchy distributions with mean 0 and scale parameter 2.5 (Gelman et al. 2008), and logit detection probability intercepts ($\beta_{0,k}$) arose from independent Normal distributions with mean 0 and variance 2. We accounted for the availability of a camera to detect moose using a trap operation matrix (effort_{ij}) for site *i* and occasion *j*, where effort_{ij} = 1 if the camera was operational and 0 otherwise. Note that we formulated the log-linear model of

abundance using sum contrasts to have the sex-specific intercepts as offsets from the overall group mean.

We derived total abundance by summing over the site-level abundance estimates and calculated the male-to-female sex ratio by dividing the estimate of adult male abundance by adult female abundance. To deal with uncertain sex status in our counts, we estimated abundance and detection probability for each sex class *k* (adult male, adult female, and unknown sex) separately and then used the proportion of males out of the combined male and female abundance estimate to partition unknown sex moose into male and female abundances.

Literature Cited

Royle, J. A. 2004. *N*-mixture models for estimating population size from spatially replicated counts. *Biometrics* 60:108–115.

Gelman, A., A. Jakulin, M. G. Pittau, and Y. Su. 2008. A weakly informative default prior distribution for logistic and other regression models. Annals of Applied Statistics 2: 1360–83.